

Biquadratic exchange in ferromagnetic/nonferromagnetic sandwiches: A spin-polarized low-energy electron microscopy study

T. Duden and E. Bauer

Department of Physics and Astronomy, Arizona State University, Tempe, Arizona 85287-1504

(Received 23 June 1998)

The magnetic domain structure of Co/Au/Co sandwich layers grown on W(110) is studied *in situ* by spin-polarized low energy electron microscopy as a function of Au spacer layer and top Co layer thickness with the goal to better understand the causes and consequences of biquadratic coupling for the resulting domain structure. It is found that biquadratic coupling not only strongly influences the coupling between the layers near the zero of the bilinear coupling but also at spacer thicknesses at which strong ferromagnetic coupling occurs. Biquadratic coupling appears in a spin reorientation transition between 4 and 5 monolayers. The existence of bilinear and biquadratic coupling produces a wrinkled in-plane magnetization. [S0163-1829(99)05601-5]

I. INTRODUCTION

It is now well established that in many ferromagnetic/nonferromagnetic thin film systems (sandwiches and superlattices) in addition to the Heisenberg bilinear exchange interaction between the magnetizations in neighboring layers also a biquadratic exchange interaction exists. The interlayer exchange energy between neighboring layers i,j is then

$$E_{ij} = J_1(1 - \cos \phi) + J_2(1 - \cos^2 \phi), \quad (1)$$

where J_1 and J_2 are the bilinear and biquadratic coupling parameters and ϕ is the angle between the magnetizations $\mathbf{M}_i, \mathbf{M}_j$ in the two layers. The biquadratic exchange is in part intrinsic, that is a property of the electronic structure of the system, in part extrinsic, that is a consequence of the geometric structure of the system. Several extrinsic mechanisms have been proposed and in part verified: nonmagnetic spacer thickness fluctuations,¹ loose spins inside the spacer or at its interfaces,² and magnetic dipole formation due to the roughness of the magnetic layers.³ The intrinsic nature of the biquadratic exchange has been demonstrated in a number of theoretical papers.⁴⁻⁹ Recent model calculations show nicely the dependence of J_2 upon spacer thickness and interface conditions.¹⁰ J_2 is oscillating like J_1 , has about twice the periodicity of J_1 , is phase shifted relative to J_1 so that maxima of J_2 approximately coincide with zeroes of J_1 and is much smaller than J_1 . The phase shift gives the possibility that the biquadratic coupling determines the magnetic structure of the system near the crossover from ferromagnetic (F) to antiferromagnetic (AF) coupling. When $J_1=0$, then $\phi = 90^\circ$ in the minimum energy configuration. This 90° coupling had led to the discovery of the biquadratic coupling by Kerr microscopy.¹¹

The fact that J_2 can be as large or even larger than J_1 in certain thickness ranges can lead to a rich magnetic phase diagram, with an asymmetric phase for large J_2/J_1 ratios.^{12,13} The goal of this paper is to explore the zero field region of this phase diagram by varying the thickness of the nonmagnetic spacer layer and of one of the ferromagnetic layers. This can be done most conveniently by imaging the magnetic domain structure during the growth of the sand-

wich by spin-polarized low energy electron microscopy [SPLEEM (Ref. 14)] in zero external field. A prototype system which had been studied by a variety of techniques before, Co/Au/Co, was chosen for this purpose. Contrary to the previous work, in which the Co layers had in general perpendicular magnetization, experimental conditions were used which lead to predominant in-plane magnetization. A strong uniaxial in-plane magnetization is obtained if the first Co layer is grown epitaxially on W(110). The out-of-plane \mathbf{M} component of this layer, which leads to a wrinkled magnetization, decreases rapidly with thickness¹⁵ and allows the simultaneous study of in-plane and out-of-plane coupling while the strong in-plane anisotropy provides a fixed reference for the coupling with the next layer.

According to previous studies of perpendicularly magnetized sandwiches the Au spacer thickness of maximum AF coupling is 5.5,¹⁶ 5.35,¹⁷ or 4.8 (Ref. 18) monolayers (ML), the second thickness with AF coupling 9.4 (Ref. 16) or 10.1 (Ref. 17) ML, with maximum F coupling in between at about 7 ML. Thus 90° coupling can be expected at about 4 ML and 6 ML but not at 7 and 8 ML unless J_2 is abnormally large. These considerations determined the Au thickness range selected. The thickness of the top Co layer was varied from 1 to 7 ML in order to cover both perpendicular and in-plane magnetization regions.

II. EXPERIMENTAL

The experiments were performed in the original LEEM instrument described in Ref. 19 in which the original field emission gun was replaced by a spin-polarized illumination system with polarization manipulator.²⁰ The base pressure of the instrument was 2×10^{-10} Torr. During the depositions the pressure stayed in the 10^{-10} Torr range and was typically around 6×10^{-10} Torr. The W(110) crystal could be heated from the back side by radiation up to 500 K and by electron bombardment up to 2000 K. It was precleaned in the preparation chamber by heating for several hours in an oxygen atmosphere at a pressure of about 2×10^{-6} Torr. Between the experiments it was cleaned regularly by annealing at approximately 1400 K in 5×10^{-7} Torr oxygen for 30 min in the preparation chamber, followed by flashing to 2000 K in

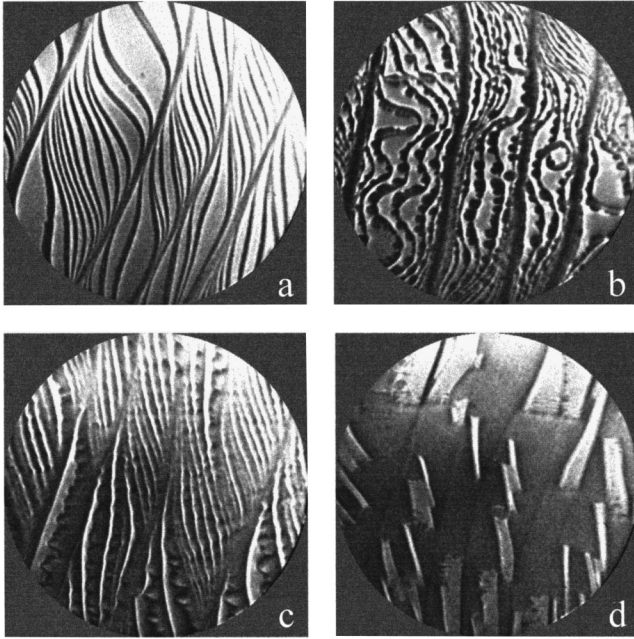


FIG. 1. LEEM images of the submonolayer growth of Co on W(110) at about 750 K. Electron energy 1.5 eV, field of view 10 μm [(a),(c),(d)] and 8 μm (b) diameter. For explanation see text.

the main chamber. Criteria for a clean surface were (i) the absence of W carbide segregation at surface imperfections upon annealing at about 1300 K and (ii) step flow growth of the first Co monolayer during the deposition at 750 K. This growth pattern is very sensitive to surface contamination by segregated or adsorbed impurities which cause pinning of the growth fronts and nucleation on the terraces. This is illustrated in Figs. 1(a) and 1(b) which show the initial growth of Co on a clean and on a contaminated surface, respectively. The first monolayer is filled in two steps: First, a pseudomorphic (ps) monolayer is formed in which close-packed (cp) islands nucleate and grow until the cp monolayer is completed. Figure 1(c) shows a typical image of an incomplete ps ML; Fig. 1(d) an image of an incomplete cp ML. The strong contrast between the uncovered W surface and ps ML regions in Fig. 1(c) and between the ps and cp ML regions in Fig. 1(d) allows a very accurate determination of the time needed to complete the ps and cp ML's. The completion of the ps and the cp monolayer provides a precise rate calibration before each experiment. After completion of the cp monolayer the temperature was reduced to about 400 K and the deposition continued to the desired thickness (7 ML). At this temperature the mobility is high enough and the two-dimensional nucleation rate low enough so that large terraces form (several 100 nm diameter) which show pronounced thickness dependent quantum size contrast. This contrast allows to observe the completion of the successively grown layers and the characterization of the Co film roughness. Once the desired Co film thickness was reached, the heating was turned off. After the temperature had decreased to values slightly above RT Au was deposited as a spacer layer. The Au deposition rate was calibrated before the Co deposition by the time needed to form 1 ML. Only the initial growth of the Au layer could be monitored via quantum size contrast. In the later stages of growth of the spacer layer the

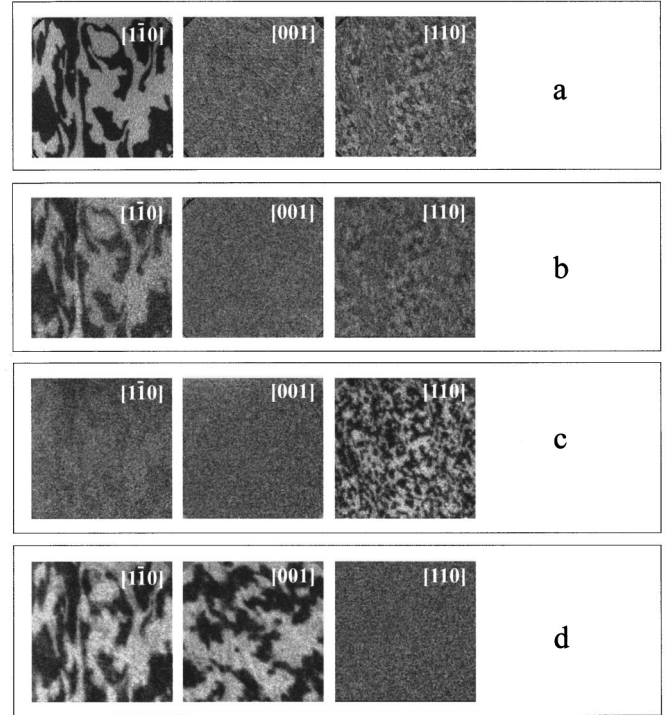


FIG. 2. Typical SPLEEM image series of a 7 Co/6 Au/7 Co/W (110) sandwich. Row (a): Uncovered bottom Co layer. Row (b): 6 Au/7 Co. Row (c): 3 Co/6 Au/7 Co. Row (d): 7 Co/6 Au/7 Co. Energy ≈ 1.2 eV; field of view here and in Figs. 5–7 approximately $6 \times 6 \mu\text{m}^2$.

contrast became very weak. On top of the stack, the second Co layer was deposited in 1 ML doses. Typical deposition rates, both of Co and Au, were 1/8 ML/min. After each monolayer dose, a measurement cycle was performed to monitor the resulting magnetic structure. The images were acquired from the final screen using a CCD camera. For each magnetic image, two images resulting from the average of 64 consecutive video frames were taken. Between each image the polarization vector of the incident electron beam was inverted. The magnetic signal was then obtained by a normalized subtraction using the formula

$$A = 127 + 100K(I_+ - I_-)/(I_+ + I_-), \quad (2)$$

where A is the normalized asymmetry, K is a contrast enhancement factor ranging from 7 to 15, and I_+ , I_- are the intensities of the images with opposite spin polarization. Due to noise the resolution in these SPLEEM images is not as good as in the original LEEM images and varies from 20 to 60 nm at the worst, depending upon the magnitude of the magnetic signal.²¹

III. RESULTS

The kind of SPLEEM images taken during the growth of the sandwiches is illustrated in Fig. 2. It shows three images for every growth stage with \mathbf{P} parallel to W [1-10], [001] and [110] from the left to the right. The [1-10] direction is the easy axis direction in the bottom Co layer. Therefore, there is no magnetic signal in the [001] image. The [110] image shows the perpendicular component of \mathbf{M} . Row (a) shows

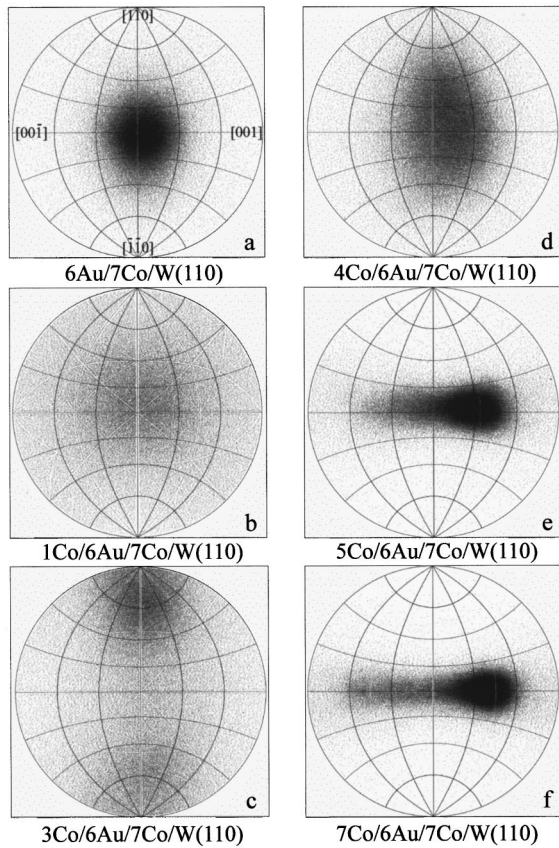


FIG. 3. Distributions of the \mathbf{M} directions extracted from the images in Fig. 2. For explanation see text.

the images of the bottom Co layer, row (b) those after deposition of 6 ML Au, row (c) those after deposition of 3 ML Co, and row (d) of 7 ML Co on top of the Au spacer. The 6 ML Au weaken the signal due to spin-independent attenuation but change neither the in-plane nor the out-of-plane \mathbf{M} component distribution [row (b)]. 1 ML Co strongly reduces the contrast and at 2 ML Co no in-plane contrast is recognizable while the out-of-plane contrast is already larger than

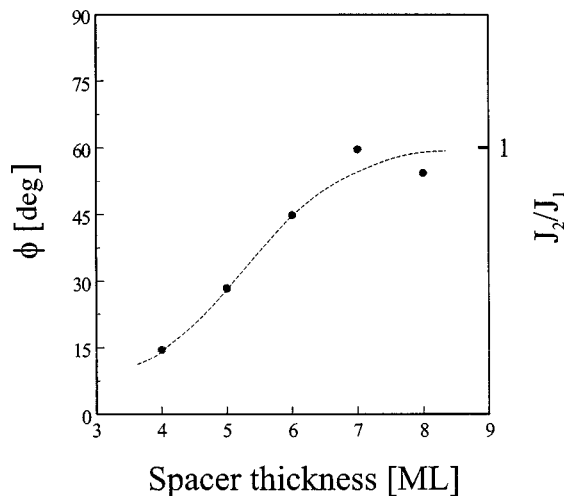


FIG. 4. Peak positions of the in-plane \mathbf{M} distribution in the completed sandwich, measured from the easy axis direction in the bottom Co layer ($W[1-10]$).

on the Au-covered Co layer (not shown). At 3 ML Co [row (c)] very weak in-plane contrast appears again and the out-of-plane contrast has its maximum intensity. It replicates the domain structure of the bottom layer perfectly in the regions in which the substrate step density is low and has much larger domains than the bottom layer in regions with high substrate step density. From 4 to 5 ML Co a dramatic change occurs: the out-of-plane contrast disappears and strong contrast is now seen in both in-plane component images ($\phi=0^\circ$, $[1-10]$ and $\phi=90^\circ$, $[001]$). This \mathbf{M} distribution does not change up to the thickest top Co layers studied [7 ML, row (d)].

The trends seen in Fig. 2 are, with minor deviations, typical for Au spacer thicknesses from 4 to 8 ML, the thickest spacer studied. In the sandwich with 3 ML Au the in-plane and out-of-plane contrast does not disappear at about 2 ML Co and develops strongly again with increasing Co thickness, completely replicating the domain structure of the bottom layer. This is probably due to F coupling through gaps in the thin Au spacer. The trends seen with the thicker spacer layers may be summarized as follows: (i) The minimum contrast in the 0° image occurs at 2 ML Co. (ii) The out-of-plane component image has maximum contrast at 3–4 ML Co. (iii) The relative contrast of the 90° and of the 0° component images increases with the thickness of the Au spacer and also somewhat with increasing thickness of the top Co layer within the thickness range studied. These trends can be quantified by calculating pixel by pixel the local direction of \mathbf{M} from the three \mathbf{M} component images and displaying them in a locally orthogonalized projection of the unit sphere. This is illustrated in Fig. 3 for the example shown in Fig. 2. The center is the 0° direction, to the left and the right are the $\pm 90^\circ$ directions and the out-of-plane directions are at the top and at the bottom. Figure 3(a) shows that the 6 ML Au have not changed the uniaxial anisotropy of the bottom Co layer. 1 ML Co (b) causes already such a strong magnetic signal attenuation that the magnetic order in the bottom layer is hardly recognizable. 2 ML Co smears out the apparent \mathbf{M} distribution even more (not shown). At 3 ML Co (c) the out-of-plane orientation is dominating but at 4 ML Co (d) there is already a significant in-plane component which leads to intermediate \mathbf{M} orientations and finally from 5 to 7 ML [(e) and (f), respectively] \mathbf{M} is completely in-plane but rotated with respect to the easy axis direction of the bottom Co layer. The angle ϕ of the maximum of the \mathbf{M} distribution in the top Co layer of the complete sandwich depends upon the thickness of the Au spacer as shown in Fig. 4. No measurements were made at 9 ML, unfortunately, so that it is not clear whether or not $\phi=60^\circ$ is the maximum value.

The coupling of the 0° component is ferromagnetic at all Au spacer thicknesses studied except at 5 ML Au where it is AF. This is illustrated in Figs. 5(a) and 5(e) for the 0° component and in 5(b) and 5(d) for the out-of-plane component. The out-of-plane image of the Au-covered bottom Co layer (b) shows only locally out-of-plane \mathbf{M} , with most of the image at the neutral grey level. The same is true after deposition of 4 ML Co but with reversed contrast corresponding to AF coupling (d). At 3 ML Co (c), however, where the out-of-plane component has its maximum, \mathbf{M} is perpendicular in the whole top layer, with AF coupling wherever there is an out-of-plane component region in the bottom layer (b). The

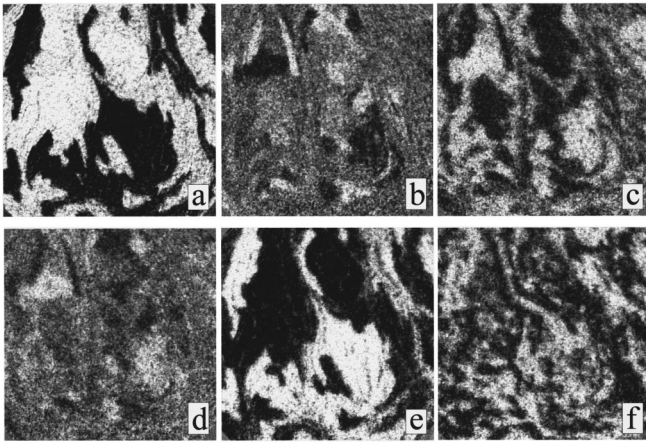


FIG. 5. SPLEEM images from various growth stages of a 7 Co/5 Au/7 Co sandwich. [(a),(b)] In-plane and out-of-plane image of the Au covered bottom layer. [(c),(d)] Out-of-plane images after deposition of 3 and 4 ML Co, respectively, on top of the Au spacer. [(e),(f)] 0° and 90° in-plane images (\parallel W[1-10] and W[001], respectively) after deposition of 6 ML Co.

development of the 90° component does not seem to depend upon the type of interlayer coupling, F or AF, as seen in Fig. 5(f) and in the dependence of ϕ upon spacer thickness (Fig. 4).

AF coupling is known to depend strongly upon the structural perfection of the spacer layer which can be varied by the deposition conditions. For this reason sandwiches with a 5 ML thick Au spacer were also prepared at elevated temperatures (≈ 400 K) at which the Au crystallites become larger and, therefore, the surface of the Au film rougher. Figure 6 shows the consequences for the magnetic structure. Figures 6(a) and 6(b) are the 0° images after Au deposition and after completion of the sandwich; Fig. 6(c) is the 90° image of the complete sandwich. There is no 0° coupling whatsoever but only a very fine-grained weakly pronounced domain structure in (b) but pronounced domains in (c). Coupling is, thus, predominantly biquadratic.

For comparison with the wrinkled magnetization in Co layers on W(110) in which the wrinkling is out-of-plane,¹⁵ Fig. 7 shows the in-plane wrinkle (d) in the top Co layer caused by the noncoincidence of the 0° and 90° \mathbf{M} distributions for a typical example, a 7 Co/6 Au/7 Co sandwich and the relation of the wrinkle to the substrate topography which is transmitted through the bottom Co layer (a). Image (d) is obtained from images (b) and (c) by calculating pixel by pixel the in-plane rotation angle ϕ and assigning to each ϕ value a grey level in the image.

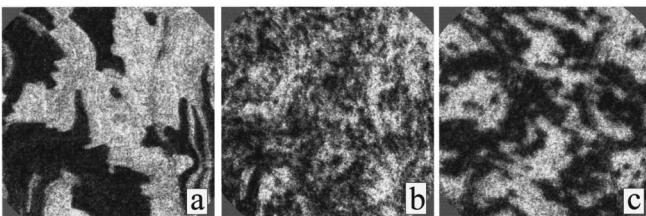


FIG. 6. Domain structure in a 7 Co/5 Au/7 Co sandwich grown at elevated temperature. (a) 5 Au/7 Co/W(110). [(b),(c)] Completed sandwich, 0° and 90° image, respectively.

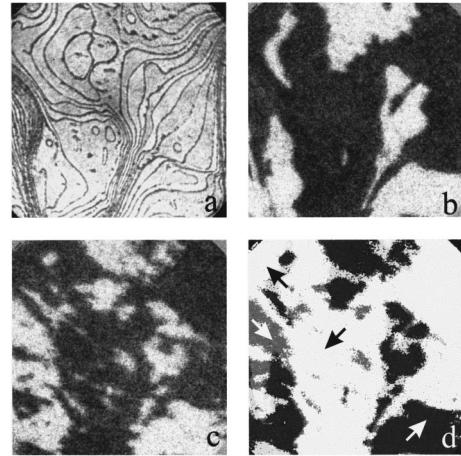


FIG. 7. Topographic image (a), 0° (b), 90° (c), and in-plane angular \mathbf{M} distribution (d) images of a 7 Co/6 Au/7 Co sandwich grown near room temperature. The four grey levels indicate the \mathbf{M} directions marked by arrows. Image (a) was taken after the deposition of the bottom Co; images (b) and (c) after completion of the sandwich. Electron energy 1.2 eV.

IV. DISCUSSION

The initial strong contrast decrease with increasing thickness of the top Co layer mentioned in Sec. III is attributed to the strong absorption of spin-down electrons in Co (Ref. 22) so that the subsequent contrast increase may be attributed to the magnetization in the top layer. The most striking results which have to be explained are (i) biquadratic coupling, that is a 90° component of \mathbf{M} , is present in all except the thinnest layer which has pure F coupling, possibly mediated by magnetic contacts through pinholes. (ii) The 90° component appears suddenly in the transition from 4 ML to 5 ML simultaneously with the disappearance of the perpendicular component, reminiscent of the spin reorientation transition (SRT) in Co layers on Au(111).²³ (iii) The parallel component always reproduces the domain pattern of the bottom layer but the 90° component has a completely unrelated domain structure which varies strongly from experiment to experiment and frequently has much smaller domains. An exception is the system grown at elevated temperature (≈ 400 K) which at the AF coupling thickness (5 ML) shows no AF coupling but only decreasing F contrast in the parallel image and increasing perpendicular contrast up to 4 ML. After the SRT at 5 ML the parallel contrast is very fine-grained while the 90° domain pattern is much more coarse-grained. (iv) The rotation of the average \mathbf{M} direction in the top layer relative to that of the bottom layer increases with Au spacer thickness; this indicates an increasing J_2/J_1 ratio because in equilibrium $\cos \phi = -J_1/2J_2$. If there is no anisotropy in the top layer, J_2 has to be larger than $J_1/2$ for \mathbf{M} to rotate.¹²

The fact that biquadratic coupling is everpresent, even close to the extrema of J_1 (5 ML and 7 ML) at which the intrinsic J_2 should be negligible, suggests that it is extrinsic. The most likely extrinsic mechanism are spacer thickness fluctuations leading to alternating F and AF coupling¹ and bipolar coupling caused by the roughness of the Co-Au interfaces.³ Bipolar coupling can not only produce a noticeable J_2 but contributes also to the perpendicular

anisotropy,^{24,25} adding to the Au/Co interface anisotropy. The largest value of ϕ in Fig. 3, $\phi \approx 60^\circ$, requires $|J_2| \approx |J_1|$, and this at 7–8 ML where J_1 has its maximum value [0.016 erg cm⁻²,¹⁶ 0.03 erg cm⁻² (Ref. 18)] so that J_2 should be about 0.02 erg cm⁻². Calculations in the free electron approximation for flat interfaces give much smaller J_2/J_1 ratios.^{4–9} Recent more sophisticated calculations of the biquadratic exchange parameters near the (100) surface of Fe, for example, give a biquadratic/bilinear ratio of about 1/6 in the close-packed directions.²⁶ *Ab initio* calculations for the system Co/Cu/Co(100) with flat interfaces and semi-infinite Co subsystems show an amplitude ratio J_2/J_1 of about 1:10.²⁷ With increasing interface roughness J_2/J_1 increases significantly. In a spacer with the average thickness of n ML consisting of about 40% n ML, 50% $n \pm 1$ ML, and 10% $n \pm 2$ ML thick regions, for example, biquadratic coupling is energetically more favorable.²⁷ In the absence of realistic intrinsic J_2 values for the Co/Au(111)/Co system only roughness will be considered here.

The bottom Co layer was prepared for optimum smoothness. The surface under these conditions is a three-level system with average terrace sizes of several 100 nm diameter made visible by quantum size contrast.²⁸ The growth of Au on this surface close to room temperature is too fine-grained to be followed via quantum size contrast. RHEED patterns of the growth of Au on Co(0001) have been interpreted as smoothing of the Co surface by the first 1.5–2 ML Au.²⁹ However, it is unlikely that the Co surface itself becomes smoother, rather the Au-covered surface by filling in the lower levels of the Co surface with Au. This is suggested by the topographic images of highly stepped regions in which chainlike contrast develops between the smaller Co islands during the initial Au deposition. Above 2 ML significant roughness develops as seen in the appearance of a RHEED transmission pattern. In LEEM this leads to the loss of topographic contrast. This suggests the model of a smooth bottom Co-Au interface and a rough top Co-Au interface, with increasing roughness in the spacer thickness range studied here. The lateral dimensions of the Au crystals are below the LEEM resolution limit which may be as poor as 50 nm under the poor contrast conditions encountered. The crystals must be at least several ML's thick in order to produce the reported RHEED pattern intensity distributions.²⁹

In any case, the Au surface is certainly rougher than the bottom Co surface, that is at least a three-level system and consists, for example at 6 ML Au thickness of at least 5, 6, and 7 ML thick regions with lateral extensions of less than 100 nm. This means that the sandwich consists of many very small AF, 90° and F coupled regions which are needed in the thickness fluctuation model of the biquadratic coupling. The observation that the 90° component appears suddenly in the transition from 4 ML to 5 ML suggests that already the 5 ML Au film has a significant 6 ML fraction. In view of this roughness the magnetic dipole mechanism probably also contributes to J_2 which is proportional to the square of the height differences.³ The \mathbf{M} distribution in the top Co layer can be obtained by vector addition of the intensities of the two in-plane component images. This was done in the same manner as previously for in-plane and out-of-plane images of Co layers on W(110).¹⁵ The result is shown in Fig. 7. This ϕ angle image is very similar to the θ angle image of Co layers

on W(110). The out-of-plane (θ) and the in-plane (ϕ) \mathbf{M} wrinkle have, however, quite different causes: competition between in-plane and out-of-plane anisotropy there, competition between bilinear and biquadratic coupling here. A microscopic model of the competition between differently coupled regions leads to the picture of static magnetization waves.³⁰

The sudden transition from the perpendicular \mathbf{M} component to the 90° (and parallel) \mathbf{M} component is a SRT which is, however, quite different from that of Co layers on thick Au(111) layers on W(110).²³ There, no 90° component is seen because there is no Co layer to couple to and the strain in the epitaxial Au layer on the W(110) surface leads to a uniaxial in-plane anisotropy. Here, the strain is assisted by the bilinear coupling while the biquadratic coupling introduces the 90° component, causing the in-plane rotation of \mathbf{M} .

The differences of the domain sizes in the out-of-plane and in-plane \mathbf{M} images have been dealt with previously:^{15,23} in-plane the monodomain is the minimum energy configuration in the absence of magnetic defects such as those caused by substrate steps; out-of-plane the striped or checkerboard pattern is preferred due to dipolar interactions. New are the domain size differences in the in-plane components. They can be accounted for as follows. The parallel \mathbf{M} component domain pattern is already present before the SRT. It is determined by the bilinear F or AF coupling with the bottom layer and, therefore, completely reproduces the bottom layer domain pattern. The SRT only increases the magnitude of the in-plane parallel \mathbf{M} component. The 90° \mathbf{M} component domain pattern on the contrary is produced during the SRT in the presence of the biquadratic coupling. Its domain size is largely influenced by roughness fluctuations which cause in-plane dipoles and corresponding \mathbf{M} direction changes. The thickness fluctuations depend strongly on the detailed deposition conditions and can change inadvertently from experiment to experiment. There is an indication of a slight domain growth with increasing top layer thickness which can be attributed to the striving for monodomain formation. The reverse situation, that is the formation of small domains in parallel \mathbf{M} and large domains in 90° \mathbf{M} during the SRT is simply due to the fact that the Au film is not continuous during the high temperature deposition as evident in the F pattern up to the SRT at the thickness at which maximum AF coupling is expected. This is an extreme case of interface roughness and thickness fluctuations so that J_2 is dominating. Under such growth conditions no AF coupling can be expected.

V. SUMMARY

We have presented a microscopic picture of how the various forms of magnetic interlayer interactions influence the magnetic domain structure of Co/Au/Co sandwiches. The results show that biquadratic coupling is always sufficiently strong in this system to have a major effect on the virgin domain structure. The spin reorientation transition in this system leads to a rotation of the magnetization of the top layer relative to that of the bottom layer by as much as 60°, indicating equal magnitude of bilinear and biquadratic exchange even at the maximum of the bilinear exchange. The extrinsic thickness fluctuation and magnetic-dipole mecha-

nism can qualitatively account for the observations. The strong biquadratic coupling contribution leads to a wrinkled in-plane magnetization in the top Co layer in which the domain boundaries are determined by substrate steps similar to the wrinkled out-of-plane magnetization in Co layers on W(110).

It should be noted that the usual methods for the study of interlayer interactions which make use of an external magnetic field cannot study the zero field line of the phase diagram. Once the system has been magnetized it cannot be brought into the zero field virgin state any more because this would require to create a huge number of domain walls.

Only when the Co films are so thin that their Curie temperature T_C is below the temperature at which structural changes occur is it possible to recover a state similar to the original one by annealing above T_C and cooling in zero field.³¹ This is rarely the case as the sample shows which was grown at elevated temperature.

ACKNOWLEDGMENT

The authors wish to acknowledge the loan of the SPLEEM equipment by the TU Clausthal, Germany.

-
- ¹J. C. Slonczewski, Phys. Rev. Lett. **22**, 3172 (1991).
²J. C. Slonczewski, J. Appl. Phys. **73**, 5957 (1993).
³S. Demokritov, E. Tsymbal, P. Gruenberg, W. Zinn, and I. K. Schuller, Phys. Rev. B **49**, 720 (1994).
⁴R. P. Erickson, K. B. Hathaway, and J. R. Cullen, Phys. Rev. B **47**, 2626 (1993).
⁵R. Bruno, J. Magn. Magn. Mater. **121**, 248 (1993); Phys. Rev. B **52**, 411 (1995).
⁶J. Barnas and P. Gruenberg, J. Magn. Magn. Mater. **121**, 326 (1993).
⁷J. Barnas, J. Magn. Magn. Mater. **123**, L21 (1993); Phys. Rev. B **52**, 10 744 (1995).
⁸J. C. Slonczewski, J. Magn. Magn. Mater. **126**, 374 (1993).
⁹D. M. Edwards, J. M. Ward, and J. Mathon, J. Magn. Magn. Mater. **126**, 380 (1993).
¹⁰J. Barnas, J. Magn. Magn. Mater. **167**, 209 (1997).
¹¹M. Ruehrig, R. Schaefer, A. Hubert, R. Mosler, J. A. Wolf, S. Demokritov, and P. Gruenberg, Phys. Status Solidi A **125**, 635 (1991).
¹²N. S. Almeida and D. L. Mills, Phys. Rev. B **52**, 13 504 (1995).
¹³T. L. Fonseca and N. S. Almeida, Phys. Rev. B **57**, 76 (1998).
¹⁴E. Bauer, in *Handbook of Microscopy*, edited by S. Amelinckx *et al.* (VCH, Weinheim, 1997), p. 751.
¹⁵T. Duden and E. Bauer, Phys. Rev. Lett. **77**, 2308 (1996).
¹⁶V. Grolier, D. Renard, B. Bartenlian, P. Beauvillain, C. Chappert, C. Dupas, J. Ferre, M. Galtier, E. Kolb, M. Mulloy, J. P. Renard, and P. Veillet, Phys. Rev. Lett. **71**, 3023 (1993).
¹⁷J. J. de Vries, W. J. M. de Jonge, M. T. Johnson, J. aan de Stegge, and A. Reinders, J. Appl. Phys. **75**, 6440 (1994).
¹⁸Y. Roussigne, F. Ganot, C. Dugautier, P. Moch, and D. Renard, Phys. Rev. B **52**, 350 (1995).
¹⁹E. Bauer and W. Teliieps, in *Surface and Interface Characterization by Electron Optical Methods*, edited by A. Howie and U. Valdré (Plenum, New York, 1988), p. 185.
²⁰T. Duden and E. Bauer, Rev. Sci. Instrum. **66**, 2861 (1995).
²¹T. Duden and E. Bauer, Surf. Rev. Lett. (to be published).
²²T. Duden and E. Bauer, J. Magn. Magn. Mater. (to be published).
²³T. Duden and E. Bauer, in *Magnetic Ultrathin Films, Multilayers and Surfaces-1997*, edited by J. Tobin *et al.*, MRS Symposia Proceedings No. 475 (Materials Research Society, Pittsburgh, 1997), p. 283 and references therein.
²⁴P. Bruno, J. Appl. Phys. **64**, 3153 (1988).
²⁵H. Szymczak, M. Rewiński, and R. Zuberek, J. Magn. Magn. Mater. **139**, 151 (1995).
²⁶D. Spisak and J. Hafner, J. Magn. Magn. Mater. **168**, 257 (1997).
²⁷V. Drchal, J. Kudrnovsky, I. Turek, and P. Weinberger, Phys. Rev. B **53**, 15 036 (1996).
²⁸T. Duden and E. Bauer, J. Electron Microscopy (to be published) (Figs. 4 and 6).
²⁹S. Ould-Mahfoud, R. Megy, N. Bardou, B. Bartenlian, P. Beauvillain, C. Chappert, J. Corno, B. Lecuyer, G. Sczigel, P. Veillet, and D. Weller, in *Magnetic Ultrathin Films: Multilayers and Surfaces/Interfaces and Characterization*, edited by B. T. Jonker *et al.*, MRS Symposia Proceedings No. 313 (Materials Research Society, Pittsburgh, 1993), p. 251.
³⁰R. Ribas and B. Dieny, Phys. Lett. A **167**, 103 (1992).
³¹M. Speckmann, H. P. Oepen, and H. Ibach, Phys. Rev. Lett. **75**, 2035 (1995).